The geochemistry and cryptic zonation of pyrochlore from San Vicente, Cape Verde Islands

N. A. HODGSON* AND M. J. LE BAS

Department of Geology, Leicester University, Leicester LE1 7RH

Abstract

Zr-rich pyrochlore crystals in carbonatite from San Vicente (Cape Verdes Islands) show cryptic, concentric and rhythmic chemical zonation with Ca increasing and Ti, U and Zr decreasing towards the rims. In one carbonatite, taken from the Camile dyke, previously undocumented cryptic sector zonation of Ti, U and Zr is also observed in these crystals. The chemical variation is investigated by wavelength-dispersive electron microprobe, with both single spot and crystal map analyses.

The concentric and rhythmic zonation, marked by element substitution, was generated by magma heterogeneity and/or element diffusion kinetics, but it is suggested that the sector zonation, marked by differential site substitution, was governed by protosite variation between octahedral and cubic faces.

KEYWORDS: pyrochlore, cryptic zonation, sector-zonation, carbonatite, Cape Verde Islands.

Introduction

THE pyrochlore group of minerals has received considerable geochemical attention, with studies of both major and minor element content and distribution (Gold, 1967; Kuz'menko, 1984; Hogarth, 1977, 1989; Knudsen, 1989). Pyrochlore crystals comprise calcium–niobium oxides and commonly occur in carbonatites as accessory minerals. Carbonatites have been reported from five of the islands in the Cape Verde archipelago, including San Vicente, Brava, Fogo, Santiago and Maio (Le Bas, 1984). Although pyrochlore has previously been noted in carbonatites from the Cape Verde Islands, only niobium-rich zirconolites from the island of Santiago have been examined in detail (Silva and Figueiredo, 1980).

This study investigates the variation in chemistry and morphology of pyrochlore in two carbonatite dykes on the island of San Vicente. The main locality sampled was the Camile dyke described by Serralheiro (1968), which represents the largest carbonatite intrusion on the island. A further sample was taken from a smaller, adjacent sovite dyke.

Carbonatite outcrop

The Camile dyke crops out 3.5 km south-east from Mindelo, the largest town on San Vicente, where the subvolcanic central igneous complex is exposed in the eroded remnants of the island-building strato-volcano. Twenty five metres north of the Mindelo-Madeiral road, the dyke forms a 5 m × 15 m outcrop orientated NE–SW. The mineral composition of the Camile dyke is dominated by fine grained irregular calcite, with accessory dolomite, apatite, baryte, iron oxides with trace pyrochlore, 'tetraferriphlogopite' and manganese oxides. The Camile dyke is interpreted to represent a calcite carbonatite showing signs of hydrothermal recrystallization.

The second pyrochlore-bearing carbonatite studied here crops out 450 m north-west of the Camile dyke, and comprises a 5 m × 5 m partially quarried dyke (Hodgson, 1985). It is comprised mainly of small calcite rhombs (up to 0.5 cm), with accessory apatite, iron oxides and trace dolomite and pyrochlore. It is interpreted as an unrecrystallized sovite with cumulate texture.

The crystals chemically analysed in this study are from two microsovitic samples of the Camile dyke (82LV51, 82LV55), and one sample of the sovite dyke (82LV43). Pyrochlore is present in only trace amounts in these samples (Nb up to 350 ppm), and comprises irregularly distributed euhedral red–brown to colourless crystals, 100–150 μm in diameter. They are typically euhedral and vary in crystal morphology from cube to cubo-octahedral (Fig. 1). The red–brown colour-

* Present address: British Gas Corporation, 59 Byranston Street, London W1A 2AZ.

Mineralogical Magazine, June 1992, Vol. 56, pp. 201–214
© *Copyright the Mineralogical Society*

ation, which correlates with the portion rich in U (18%), is interpreted to represent crystal lattice damage from radioactive decay of uranium; however the crystals are entirely isotropic.

Analytical techniques

This study aimed to investigate the cryptic chemical variation within the pyrochlore in two carbonatites from San Vicente. They were analysed using the Cambridge Instruments Microscan 9 wavelength dispersive electron microprobe, at the British Museum (Natural History), London. Raw data were ZAF corrected on line. The results were calibrated relative to natural and synthetic standards, and spectral interferences, including those for the rare earth elements, were computed from the analysis of the standards.

In Table 1, eight analyses of pyrochlore from the calcite carbonatite of the Camile dyke are presented, all from sample 82LV51 (crystals A, B, C), also four from crystal D of pyrochlore from the sovite dyke sample 82LV43. Fluorine and chlorine abundances were investigated in crystals A, B and C in sample 82LV51 in a separate set of wavelength-dispersive analyses performed on the Cambridge Mark 5 electron microprobe at Leicester University. Each analysis presented comprises an average of three determinations of the major constituents (Na_2O, CaO, TiO_2, ZrO_2, Nb_2O_5 and UO_2) for a given spot. Relative to other pyrochlore analyses (e.g. Hogarth, 1989),

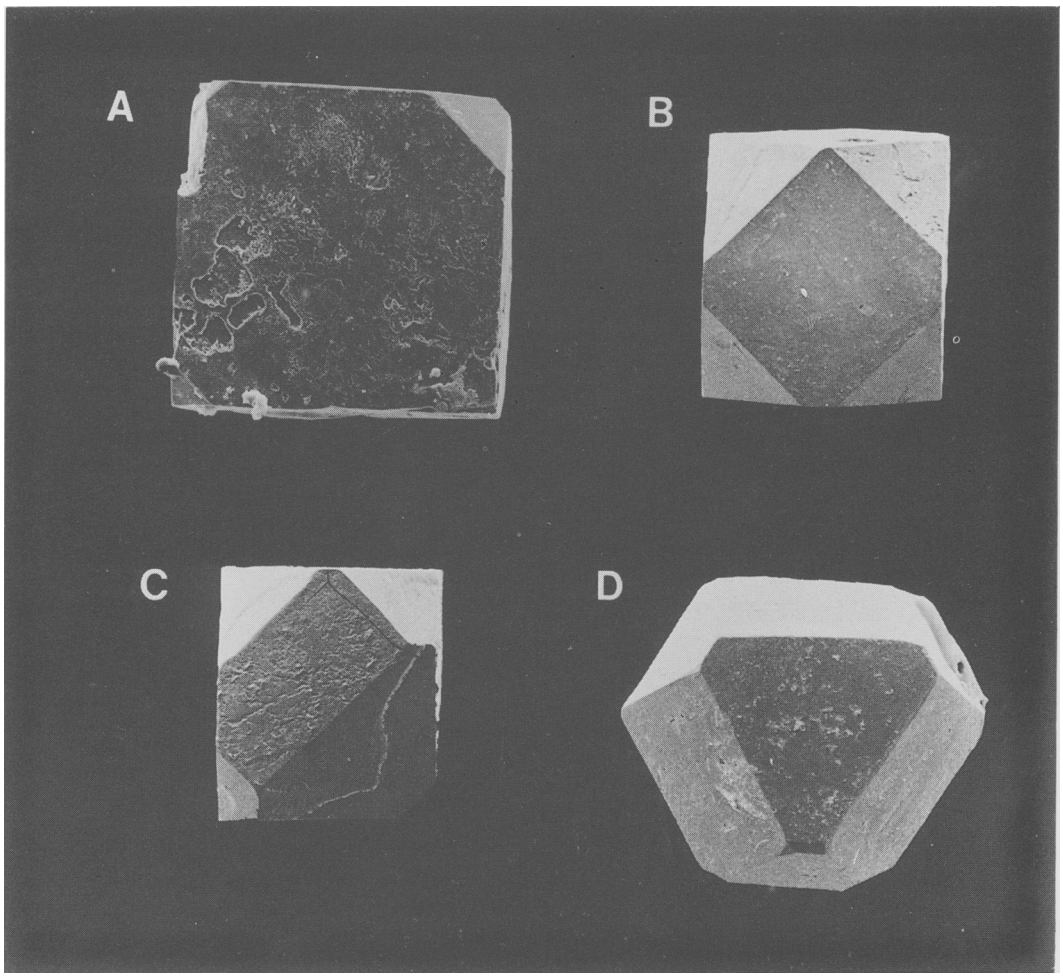

FIG. 1. Scanning electron photomicrographs of cube and cubo-octahedral crystals of pyrochlore hand-picked from the residue of 82LV51 after acid (HCl) attack. Crystal A is 150 μm across. D is from 82LV43.

Table 1: Wavelength dispersive pyrochlore analyses (weight %)

Sample	82LV51	82LV51	82LV51	82LV51	82LV51	82LV51	82LV51	82LV51	82LV43	82LV43	82LV43	82LV43
Crystal	A	A	A	B	B	B	C	C	D	D	D	D
Analysis	A1	A2	A3	B1	B2	B3	C1	C2	D1	D2	D3	D4
Na2O	5.39	2.13	5.23	4.82	5.46	4.95	4.69	5.52	5.69	6.37	6.07	3.58
CaO	16.96	11.01	17.84	18.79	17.48	18.38	18.23	17.21	13.99	17.17	17.23	14.04
UO2	13.07	16.35	9.79	7.77	11.94	8.79	8.81	11.63	16.83	0.83	0.28	9.69
TiO2	7.5	7.31	5.14	4.49	7.56	4.7	4.11	6.97	4.11	2.2	2.05	3.59
ZrO2	5.07	4.31	8.34	9.76	4.63	9.13	10.25	4.5	5.53	3.75	3.62	5.31
Nb2O5	47.79	47.69	49.38	50.31	49.28	50.52	49.78	50.02	49.63	60.55	62.98	54.47
Fe2O3	0.27	0.31	0.16	0.09	0.27	0.14	0.11	0.29	0.38	0.24	0.23	0.49
La2O3	0.19	0.59	0.22	0.38	0.27	0.25	0.24	0.17	0.22	0.32	0.4	0.44
Ce2O3	0.77	0.87	0.91	1.14	0.88	1.1	1.11	0.8	0.95	2.28	1.95	1.7
Pr2O3	0.14	0.35	0.19	0.14	0.14	0.18	0.16	0.19	0.17	0.18	0.18	0.12
Nd2O3	0.3	0.41	0.3	0.3	0.16	0.3	0.3	0.2	0.27	0.51	0.46	0.4
Sm2O3	b.d.	0.13	b.d.	0.13	0.09	b.d.	0.21	0.12	0.05	0.21	0.09	0.13
Gd2O3	0.19	0.17	0.23	0.06	0.12	0.36	0.17	0.05	0.19	0.39	0.23	0.2
Yb2O3	0.05	b.d.	b.d.	b.d.	0.08	0.02	0.1	b.d.	b.d.	b.d.	0.02	0.03
Y2O3	0.08	0.06	b.d.	0.04	b.d.	0.02	0.06	0.02	0.05	0.1	0.09	0.12
SiO2	0.94	2.41	0.22	0.11	0.83	0.15	0.13	0.67	0.22	0.09	0.11	0.71
HfO2	0.11	0.26	0.26	0.11	b.d.	0.08	0.05	0.02	b.d.	0.05	0.05	0.21
Ta2O5	0.27	0.37	b.d.	0.3	b.d.	0.4	0.02	0.24	0.21	b.d.	0.21	0.13
ThO2	1.03	0.55	0.89	0.93	0.96	0.87	1.01	1.09	1.4	1.89	1.91	2.82
K2O	0.03	0.12	0.05	0.04	0.02	0.04	0.04	0.03	0.06	0.04	0.05	0.07
SrO	0.32	1.46	0.4	0.48	0.29	0.44	0.45	0.32	0.26	0.47	0.49	1.21
BaO	0.15	0.41	0.11	0.07	0.19	0.11	0.13	0.19	0.13	0.04	0.04	0.63
Al2O3	n.a.	n.a.	n.a.	n.a.	n.a.	n.a.	0.02	b.d.	n.a.	n.a.	n.a.	n.a.
MnO	n.a.	n.a.	n.a.	n.a.	n.a.	n.a.	0.03	0.04	n.a.	n.a.	n.a.	n.a.
MgO	n.a.	n.a.	n.a.	n.a.	n.a.	n.a.	b.d.	0.04	n.a.	n.a.	n.a.	n.a.
PbO	0.38	0.98	0.23	0.32	0.28	0.2	0.13	0.3	0.17	0.51	0.39	0.93
TOTAL	101	98.25	99.89	100.59	100.93	101.13	100.34	100.63	100.51	98.19	99.13	101.02
F	2.24	2.39	2.58	2.57	2.73	2.34	2.59	2.57	n.a.	n.a.	n.a.	n.a.
Cl	0.03	0.02	0.01	0.01	0.01	0.04	0.01	0.01	n.a.	n.a.	n.a.	n.a.
-O=F	-0.93	-0.99	-1.07	-1.07	-1.13	-0.98	-1.08	-1.07	—	—	—	—
TOTAL	102.34	99.67	101.41	102.1	102.54	102.53	101.86	102.14	—	—	—	—
Na+	5.63	2.26	5.36	4.84	5.54	4.98	4.76	5.7	6.26	6.41	5.93	3.71
Ca2+	9.81	6.45	10.13	10.45	9.92	10.24	10.23	9.84	8.51	9.56	9.32	8.06
U4+	1.57	1.99	1.15	0.9	1.41	1.02	1.02	1.38	2.15	0.1	0.03	1.15
Ti+	3.03	3.08	2.04	1.75	3.02	1.83	1.62	2.79	1.75	0.86	0.78	1.44
Zr4+	1.33	1.15	2.15	2.47	1.2	2.32	2.62	1.17	1.53	0.95	0.89	1.39
Nb5+	11.63	11.77	11.8	11.78	11.79	11.85	11.77	12.04	12.72	14.19	14.33	13.17
ΣA	17	10.7	16.64	16.19	16.89	16.24	16.01	16.92	16.92	16.06	15.27	12.93
ΣB	16	16	16	16	16	16	16	16	16	16	16	16
Σ(+)	112.04	108.63	108.99	107.98	110.74	108.53	107.77	111.07	112.26	109.37	107.24	109.04

b.d. : below detection

n.a : not analysed

the totals of the analyses in Table 1 are high, especially in analyses indicating high UO_2 and Na_2O. This may reflect errors incurred during the ZAF count data reduction process (Hogarth, pers. comm., 1989).

In addition to single spot elemental analyses, the intra-crystalline cryptic variation of major elements was investigated by generating wavelength-dispersive X-ray scanning image photographs, 'elemental distribution maps'. These maps of geochemical variation within single crystals allow the observation of oscillatory, multiple and sector zoning within the San Vicente pyrochlore crystals (Figs. 2 and 3).

The bulk rock and rare earth element chemical analyses were obtained by normal XRF and INAA procedures at Leicester University (Hodgson, 1985).

Classification

Members of the pyrochlore group are classified as 'multiple cubic oxides, bearing essential Nb, Ca and Ti, individually and in combination' (Hogarth, 1977). They have the space group *Fd3m* and have the general formula:

$$A_{16-m}B_{16}O_{48}(O,OH,F)_{8-n}.pH_2O \qquad (1)$$

where A represents the 16*d* site (= the *A*-site), *B* represents the 16*c* site (= the *B*-site), and '*m*' and '*n*' represent vacancies in the unit cell, '*p*' represents bound water molecules. *m*, *n* and *p* are not rational.

The *A*-site is considered to hold Ca, Na, As, Cs, Mg, Sb, Th, Mg, Y, K, Mn, Sr, Fe^{2+}, Sn, Ba, *REE*s, Pb, Bi and U, whilst the *B*-site consists of a six-fold site bearing Nb, Ta, Ti, Mn and Fe^{3+} (Petruk and Owens, 1975; Hogarth, 1989). The location of Zr and Si in the pyrochlore structure is currently unclear and will be discussed below.

The crystals analysed here are considered to be true pyrochlores because molecular (Nb + Ta) > 2Ti and Nb > Ta, but it is possible that they could represent pseudocubic members of the zirconolite group. However the Zr content is much lower than in zirconolite, and the Na_2O content (Table 1) of the crystals is greater than that of natural zirconolites, which reach only up to 1.40% Na_2O (Borodin *et al.*, 1960), and synonymous synthetic zirconolites have only up to 2% (Kesson and Ringwood, 1981). Additionally, the analyses in Table 1 display very low Ti (relative to the betafite group) and very low Ta (relative to microlites and hatchettolite). Following the IMA Pyrochlore Subcommittee recommendations (Hogarth, 1977), the pyrochlore analyses presented in Table 1 are thus all classified as pyrochlore species. Confirmatory X-ray diffraction analysis to determine if these crystals are cubic (pyrochlore) or pseudo-cubic (zirconolite) has not been possible owing to lack of material.

Crystallographic site discussion

The geochemistry of the pyrochlores is discussed by reference to the pyrochlore unit cell formula, where elements weight % (wt.%) are normalized to a *B*-site occupancy of 16 (Table 1). The rationale for this is that pyrochlore is thought to bear vacancies only in the *A*-site (Borodin and Nazarenko, 1957; Petruk and Owens, 1975; Hogarth, 1989). Thus the formula unit for any element may be calculated by normalizing to the simplified total *B*-site occupancy of 16 formula units. The assignation of site occupancy of the Zr atoms is critical in this normalization, because included in the analyses in Table 1 are examples where the ZrO_2 contents are higher than for any previously published pyrochlores (e.g. 4.1 wt.% of Perrault, 1968; 3.0 wt.% Lebedeva *et al.*, 1973). The balance of *A*-site for *B*-site atoms is possible only if the Zr atoms from these analyses are assigned to the *B*-site. Therefore *B*-site = atomic (Nb + Ti + Zr) = 16.

Simplifying the total *A*-site occupancy to atomic (Na + Ca + U) and normalizing to 16 *B*-site units, the *A*-site of the analyses are found to be nearly always greater than 16 (see Table 1), although never by more than 6.0%. Analytical error or count data reduction errors are possible, but Fig. 4 suggests this is unlikely. Additional elements potentially substituting into the *B*-site are Ta, Al, Si, Fe^{3+} and Mn. As the abundances of Ta, Al and Mn are very low, it follows that including these elements into the *B*-site cannot reduce *A* to less than 16. Adding Si and Fe^{3+} to *B*-site atoms would permit normalization of *A* to less than 16 (Knudsen, 1989). However this has been resisted owing to the considerable uncertainty in the site assignation of these elements, although the element distribution maps (Fig. 2) seem to offer support for Si in the *B*-site.

The total charge in the *A*- and *B*-sites of the unit cell has been calculated for the analyses given here. It is found to lie within a range from +107.24 to +112.26. In the pyrochlore unit cell, these charges are balanced by F^- ions (sample 82LV51 measured range −3.39 to −4.59), OH^- ions (range −56 to −48) and O^{2-} ions (range −48 to −(56-F-OH); equation 1). In sample 82LV51, three of the analyses (all high Na, high U) have total *A* + *B* site charges greater than can be balanced by O^{2-} ions with the measured F content.

Quantification of the intra-site substitutions is made possible by studying the element distributions in the *A* and *B* sites for the crystal zones analysed. Due to the variation in the ionic radius and ionic charge of the major elements, coupled substitutions between *A* and *B*-sites are required to balance cell size and site charge. Substitutions suggested by Hogarth (1989) for the development of uranium-rich pyrochlore are;

$$Ca^{2+} + 2Nb^{5+} = U^{4+} + 2Ti^{4+} \text{ (betafite scheme)} \quad (2)$$

or

$$2Ca^{2+} = U^{4+} + \square \text{ (uranopyrochlore scheme)} \quad (3)$$

where □ is a vacant *A*-site. A plot of atomic Nb *vs.* U is given in Fig. 4A. This shows that, although there is significant variation in atomic U in the analyses from 82LV51, the variation in Nb is within the error of analysis, and would seem to suggest that the substitution operating during the growth of the 82LV51 is not that described by equation 2. But if analysis A2 is ignored (see below where A2 is shown to be part of an alteration rim), then within the scatter of the data one could interpret that as U–Nb exchange, although the betafite scheme does not operate. In 82LV43 however, the four analyses of crystal D provide support for U–Nb substitution (Fig. 4A).

For the *A*-site element substitutions, a plot of U *vs.* Ca (Fig. 4B) shows a trend in composition from analyses A1 and B2 to analyses B1 and B3 (all from 82LV51). The slope of this correlation indicates a 1:1 exchange of Ca for U. The plot for 82LV43 (Fig. 4A) lends support for this exchange. The variation of Na with U in 82LV51 crystals is positively correlated with a slope between 2:1 and 1:1 (Fig. 4C), indicating a linked exchange of Na and U, as well as coupled *A* and *B* site substitution (equation 2). The ion exchange relation suggested by these correlations

$$Ca^{2+} = U^{4+} + Na^{+} \quad (4)$$

neither balances charge nor formula units in the *A*-site. A conjectured but unlikely alternative is that coupled substitution of unanalysed negative ions may occur (e.g. O^{2-} substituting for OH^{-}), and hence that there may be fluorine variation in excess of that actually measured in 82LV51:

$$Ca^{2+} + \square + 3(OH^{-}, F^{-}) = U^{4+} + Na^{+} + 3(O^{2-}). \quad (5)$$

However, even this alternative model is fraught with problems, as the variation in fluorine that would be required would be in the order of 1.5 to 2 wt.%. Additionally, systematic variation in fluorine is not observed in 82LV51 and, as discussed above, the high positive summation does not allow much freedom in OH^{-}, F^{-} substitution for O^{2-} (Table 1). Significant site and charge imbalance during *A*-site element substitution is inferred from the relationships in Fig. 4. It is not yet clear how the pyrochlore unit cell accommodates these imbalances.

The oxidation state of uranium in these pyrochlores remains unclear. It is reported in Table 1 as U^{4+} in line with previous studies. Attempting to reduce charge balance equations to resolve the U^{3+}/U^{4+} question is not effective, as it would be necessary to allow for unmeasured O^{2-}, OH^{-}, and F^{-} in the pyrochlore structure. The suggestion that uranium may be in the 3+ state, allows a substitution of the order:

$$Ca^{2+} + \square + 2(OH^{-}, F^{-}) = U^{3+} + Na^{+} + 2(O^{2-}). \quad (6)$$

The discussion of site substitutions in these pyrochlores is hampered by this lack of constraint on the oxidation state of uranium, also by the uncertainty on the site assignation of Zr, Si and Fe, the lack of OH analysis and the limited number of full analyses. Additionally there is the possibility that the analyses (especially with high Na and U) are effected by minor errors due to the inability of the ZAF program to reduce the count data accurately for these elemental compositions. Therefore a fuller and more meaningful discussion of the possible major element substitutions operating in the *A*-site during the growth of the pyrochlore in 82LV51 cannot be taken further.

B-site substitution in 82LV51 is restricted to that of Ti for Zr (Fig. 4D). There is no evidence for Nb substitution. As Ti and Zr are negatively correlated with a slope of −1, a mutual substitution is indicated. Such a relationship is observed on the corresponding element distribution maps (Fig. 2). This substitution is related to that observed in the *A*-site as the trend again follows from analyses A1 and B2 (U + Na-rich) to analyses B1 and B3 (Ca-rich). It is suggested that the distortion of the crystal lattice caused by substitution of uranium into the *A*-site, and the concomitant contraction of the *B*-site leads to the preferential exclusion of Zr^{4+} relative to the smaller Ti^{4+} ion.

An alternative suggestion to resolve the charge and site balance problem is that Zr should be assigned fully or in part to the *A*-site. The major obstacle to this solution is that this would require that either another *A*-site element to fill a *B*-site position, or that the *B*-site displays vacancies. Both of these conditions are considered unlikely (Hogarth, 1989).

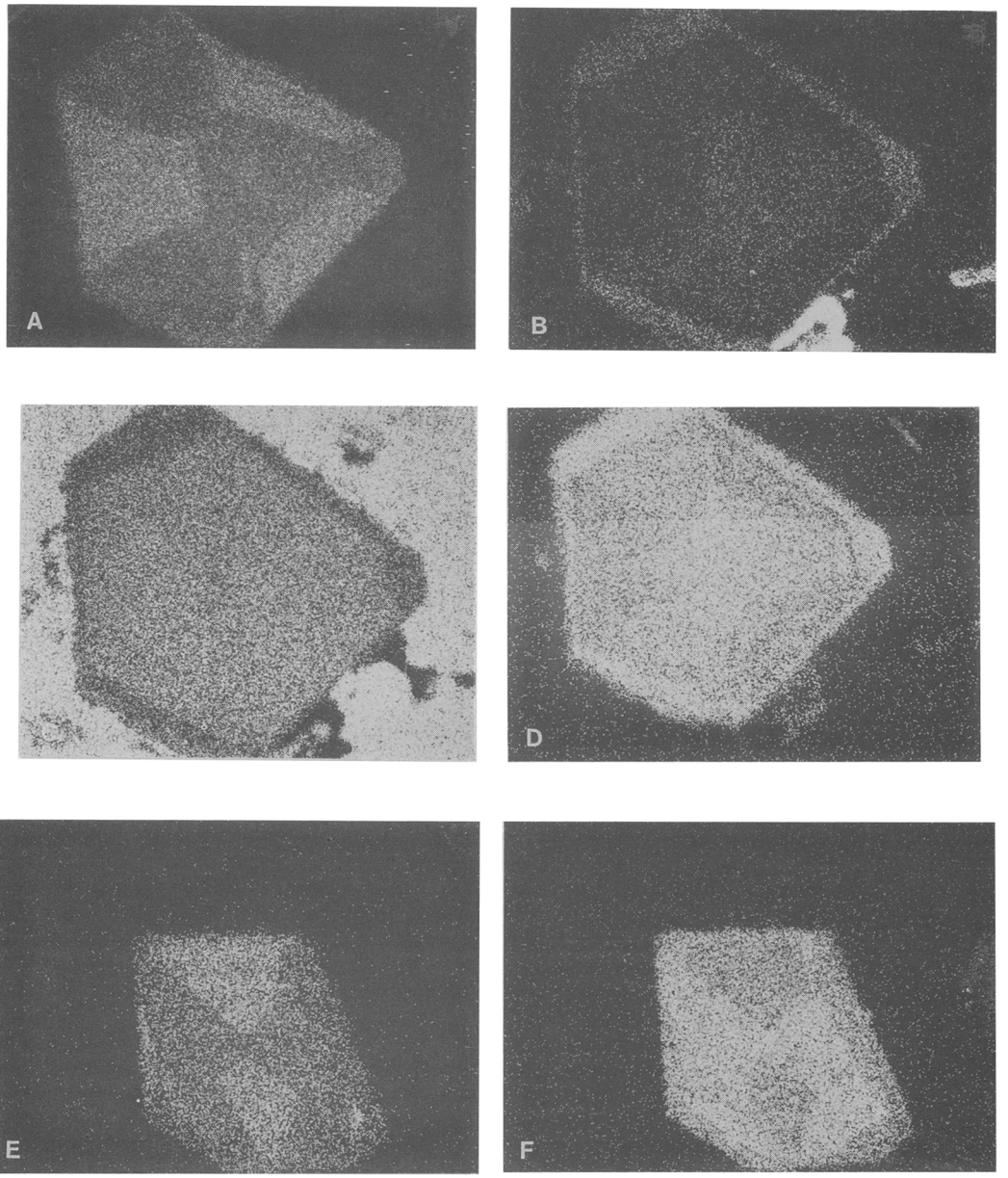

FIG. 2. X-ray scanning and back-scatter photomicrographs showing element distribution of pyrochlore crystals in carbonatites 82LV51 (A–F), 82LV55 (G–J) and 82LV43 (K, L): *A*—crystal A, Zr sector zonation; *B*—crystal A, Si sector zonation poorly developed, but with Si-rich rim; *C*—crystal A in calcite, Ca-poor rim; *D*—crystal A, U sector zonation and U-rich rim; *E*—crystal B, Zr sector zonation; *F*—crystal B, Ti sector zonation.

Conclusive demonstration of the elemental substitutions within pyrochlore from the sovite dyke (82LV43) is restricted by the limited number of analyses taken. Fig. 4 indicates that the chemical lattice substitutions in both the *A* and *B* sites of the crystals from the sovite dyke are dissimilar from those occurring during the development of pyrochlore from the Camile dyke. For example, Fig. 4D indicates that there is positive correlation between Zr and Ti substitution in the pyrochlore from the sovite. This is correlated with Nb depletion, suggesting charge balancing of *A*-site substitutions by *B*-site substitution of Nb^{5+} for $[Ti, Zr]^{4+}$. The substitution mechanisms occur-

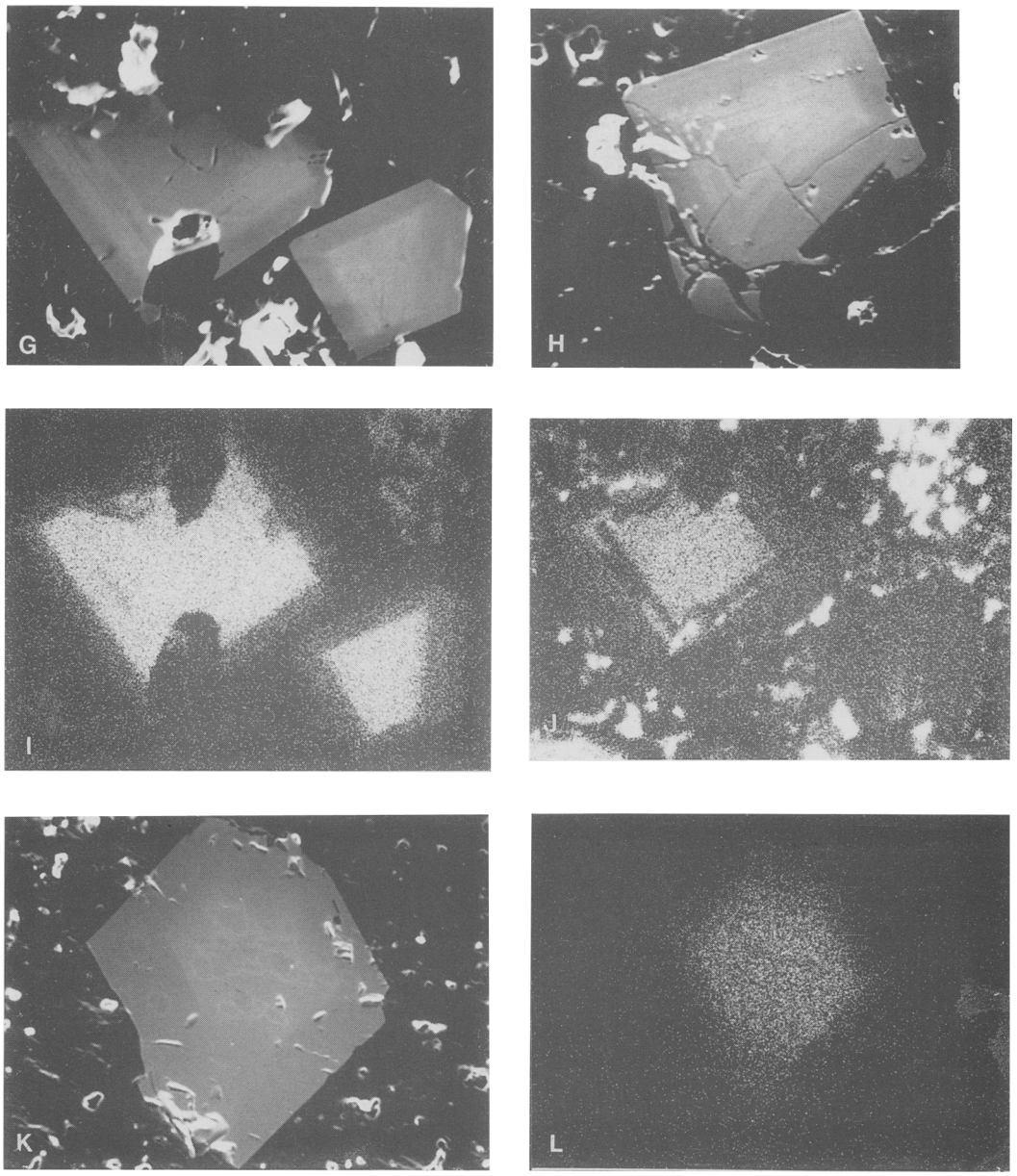

FIG. 2—continued: *G* and *H*—backscatter of two cubo-octahedral crystals showing rhythmic zoning; *I*—crystals shown in G above with U-rich cores; *J*—another crystal as in G showing Si-rich core; *K*—crystal D, backscatter showing octahedral form; *L*—crystal D, U-rich core. Scale: each photograph is 175 μm across.

ring during the growth of these crystals apparently differed from those in the crystallization of the Camile dyke (82LV51). This may be related to the lack of sector zoning in the pyrochlore from the sovite dyke.

Analysis A2, taken at the edge of crystal A in 82LV51, shows a different chemical signature from the other analyses in 82LV51 (see Figs. 4B, C). In terms of *A*-site occupancies, analysis A2 has some similarities with the U-rich core of crystal D (analyses D1 and D4, Table 1). Such U-rich cores are evident in X-ray scanning imagery (Figs. 2I, J) of the pyrochlore crystals in 82LV55, and this appears to be the norm for most other

carbonatitic pyrochlores in the world (Hogarth, 1989). The *A*-site depletion in Na and Ca and enrichment in U and Si in the outer zone of crystal A is, on the evidence of the rare earth element (*REE*) content discussed below, taken to indicate that late-stage or secondary alteration can cause exchange and depletion of the *A*-site elements.

Geochemistry

The host rocks, 82LV43, 51 and 55, have the characteristic bulk chemical composition of average carbonatites. This is demonstrated by the primordial mantle-normalized element distribution plot (Fig. 5) which shows ratios that fall within the range of calcio-carbonatites elsewhere (Woolley and Kempe, 1989), particularly by the characteristic peaks of Ba, Nb and *REE*s. The three samples are also chemically similar, but 82LV55 can be distinguished as the least fractionated of the three, having relatively low Ba and high Nb, P and Zr, while 82LV43 is more fractionated, having relatively higher Ba and lower Nb, P and Zr. The chondrite-normalized *REE* plots (Fig. 6) show the characteristic smooth distribution patterns and steep ratios (La/Yb_N *c.* 33) typical of carbonatites. Furthermore, Ce anomalies are absent, confirming the lack of

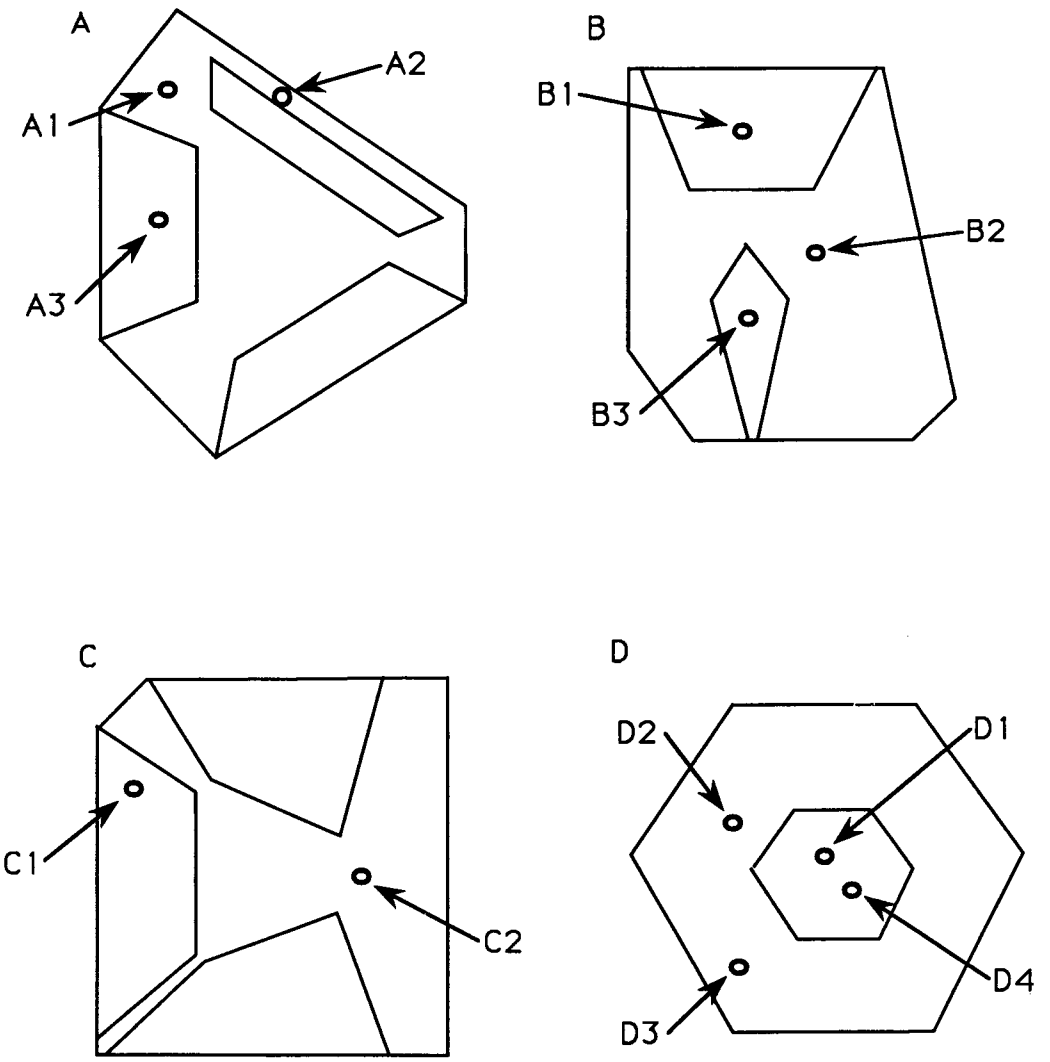

FIG. 3. Sketches showing positions of points microprobe analysed relative to the sector zonation and cryptic zonation. *A*, crystal A of 82LV51; *B*, crystal B of 82LV51; *C*, crystal C of 82LV51; *D*, crystal D of 82LV43.

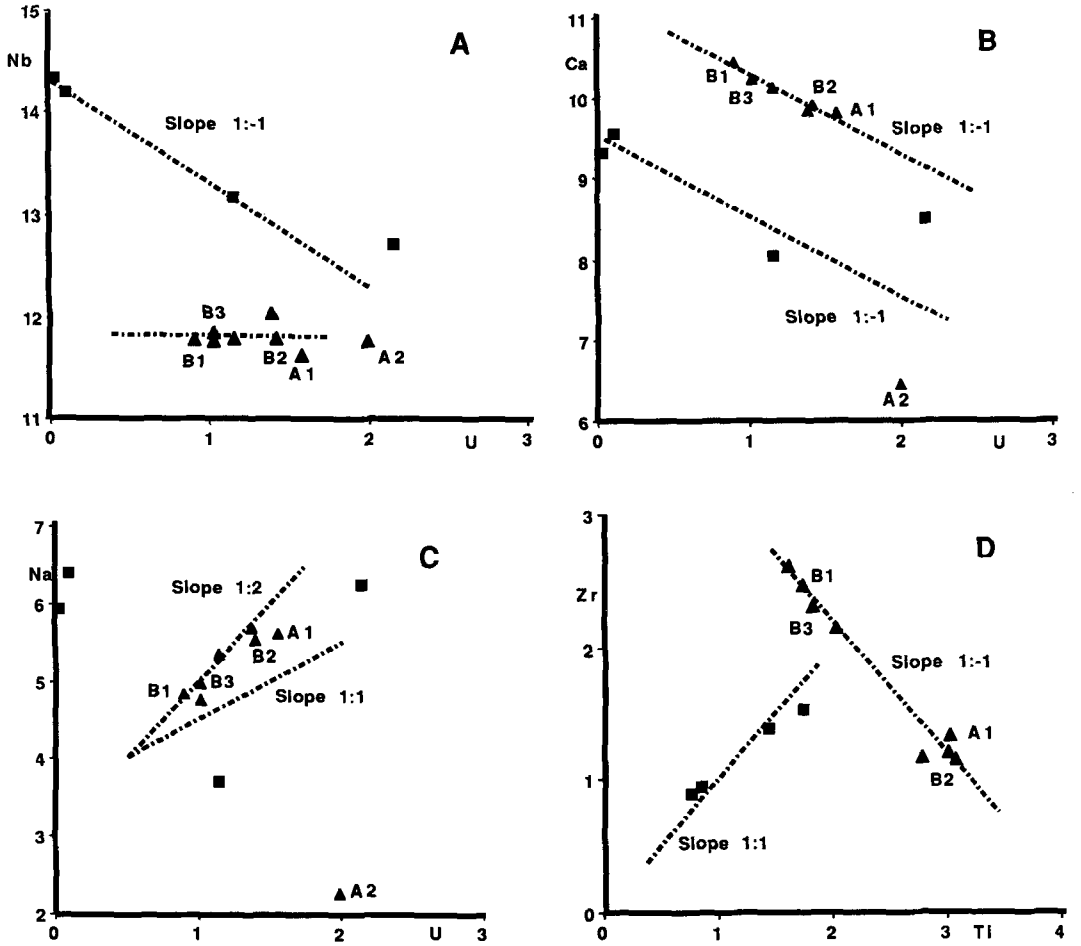

FIG. 4. Elemental formula units normalized to 16 *B*-site occupancies for pyrochlores 82LV51 (triangles) and 82LV43 (squares); *A*, U *vs.* Nb; *B*, U *vs.* Ca; *C*, U *vs.* Na; *D*, Ti *vs.* Zr.

appreciable secondary alteration. The reason for the flattening of the curves at the heavy *REE*s is not understood at present; it is not thought to be an analytical artifact.

The rare earth data for the pyrochlore crystals in the carbonatites given in Table 1, are shown chondrite-normalized and averaged on Fig. 7. They have similar *LREE/HREE* ratios but different distributions of La, Ce and Pr from those of the host carbonatites. The pyrochlores of 82LV43 are *RE*-enriched compared with those from 82LV51, in keeping with the observation made from Fig. 5 that 82LV43 is more fractionated than 82LV51. The positive anomaly in the *LREE* pattern for Ce is common in carbonatitic pyrochlore analyses, e.g. at Oka, Canada and Kaiserstuhl, Germany (Hogarth, 1989), but the enrichment of Pr remains unexplained.

The *REE* content of analysis A2 is different from the other pyrochlore analyses, and is plotted separately, with error bars, on Fig. 7. It shows a steeper *LREE/HREE* pattern, peaking at Pr, and with a negative Ce anomaly. A negative Ce anomaly is usually attributed to oxidation of Ce^{3+} to the Ce^{4+} state, and selective removal by fluids. Analysis A2 comes from the edge of crystal A in 82LV51 (Fig. 3A), and that same analysis also shows an abnormal deficiency of *A*-site atoms, seen in the low contents of Na and Ca in the analysis in Table 1. Na would also be prone to removal by fluids. X-ray scanning image photographs also show the edge of crystal A to be enriched in Si and U (Fig. 2B, D). Normally Si and U are enriched at the core of pyrochlore crystals and impoverished at the margins (Fig. 2I, J, L). Therefore, the unique chemistry at the

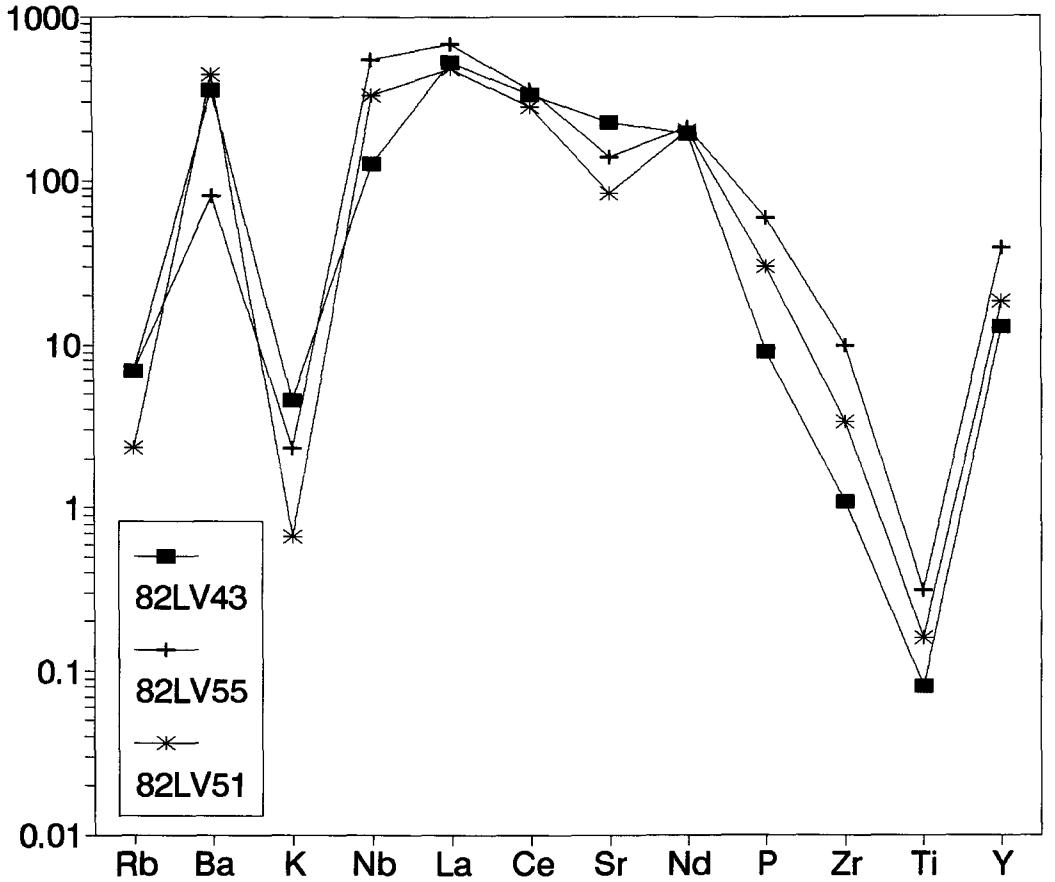

FIG. 5. Primordial mantle-normalized element distribution ratios for carbonatites 82LV43, 51 and 55 from San Vicente, Cape Verde Islands (XRF analyses).

margin of crystal A is best explained by minor late-stage or secondary alteration, which belongs to a separate process from the fractionation being discussed here.

Discussion of cryptic geochemical zonation

Concentric zoning is well known in pyrochlore and Nb-Ti minerals (Vronskii and Basina, 1963; McMahon and Haggerty, 1979; Petruk and Owens, 1975) but sector zoning, which is present in pyrochlore crystals A, B and C from 82LV51, has not previously been recorded.

The relationship between chemistry and crystallographic orientation has been investigated by combining the results of the elemental distribution imagery maps (Fig. 2) with wavelength-dispersive microprobe analyses. Samples from both the sovite dyke and the Camile dyke have well displayed concentric zonation of U, Ti, Ca, Zr and Si, with fine oscillatory rhythmic zonation of U and Si only just visible on Figs. 2G and H. Elements U, Ti, Zr and Si are more concentrated towards the cores, while Nb, Ca and Na increase towards the margins. The zoning may in part be controlled by pressure, temperature, growth rate versus elemental diffusion rate and volatile activity variation during crystal growth.

Growth of pyrochlore crystals could locally and rapidly deplete their host fluid of niobium and uranium, developing short-lived chemically heterogeneous domains. The homogenization of these domains would replenish the host fluid with Nb and U, and repetition of this process during emplacement could produce the concentric and rhythmic zonation observed. However, carbonatitic magma has low viscosity and would flow turbulently during emplacement, especially in relatively thin dykes (Treiman, 1989; Hodgson, 1985). Under such turbulent flow the re-equilibration of such domains would be rapid (Treiman

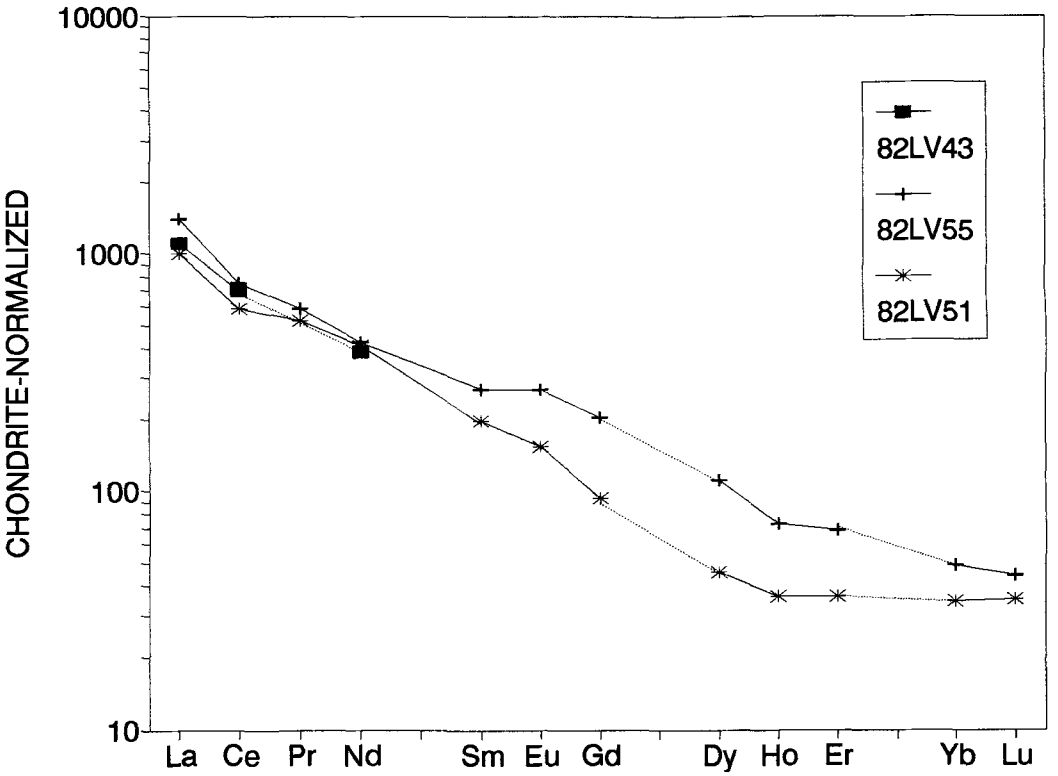

FIG. 6. Chondrite-normalized rare earth element distribution ratios for carbonatites 82LV43, 51 and 55 from San Vicente, Cape Verde Islands (82LV43—XRF; 82LV51, 55–ICP).

and Schedl, 1983). Therefore crystal growth would be unlikely to deplete the magma at a rate that exceeded magma homogenization. Instead, it is envisaged that the crystals grew during gravitational settling or during circulation within a chemically stratified magma chamber. Less likely would have been cyclic changes in volatile pressures during crystal growth.

In cases when the conjugate fluid was not replenished, for example in a consolidating crystal mush as in sovite cumulate 82LV43, the concentric zonation of the pyrochlore crystals would not be expected to be rhythmic but to represent a depletion profile. In pyrochlores from sovite 82LV43, this process may explain the simple development of a U-rich core surrounded by a U-poor rim (Fig. 2L).

Study of the sector zoning observed in thin section where crystals are irregularly oriented, is helped by creating a 3-D geometric model of the distribution of the sector zones. The model (Fig. 8) indicates the relation of the images in Figs. 2 and 3 to the crystallographic axes, and of the elemental distribution maps of crystals displaying both cubic and octahedral faces. Figs. 2A, B, C and D are taken sub-parallel to the (111) face. Only pyrochlores in carbonatite 82LV51 show sector zoning, with Zr enriched on the cube faces, and U, Ti, and Si enriched on the octahedral faces. Only Zr, U and Ti are illustrated (Figs. 2A, D, E and F).

Rapid crystal growth relative to ionic diffusion, such that the growth rate is greater than the rate of element supply, can produce sector zoning in clinopyroxenes (Wass, 1973). Applying this model to pyrochlore crystals A, B and C of 82LV51, would invoke preferential incorporation of elements such as U and Ti on to the [111] axis as a result of rapid crystal growth relative to the diffusion of U and Ti. Such a process would operate throughout the Camile dyke, presuming that the magma in the dyke crystallized at broadly similar compositions and at similar pressures and temperatures, and in such circumstances pyrochlore crystals elsewhere in the dyke would have grown at similar absolute growth rates. However, the crystals in sample 82LV55, located in the Camile dyke 0.75 metres from 82LV51, do not

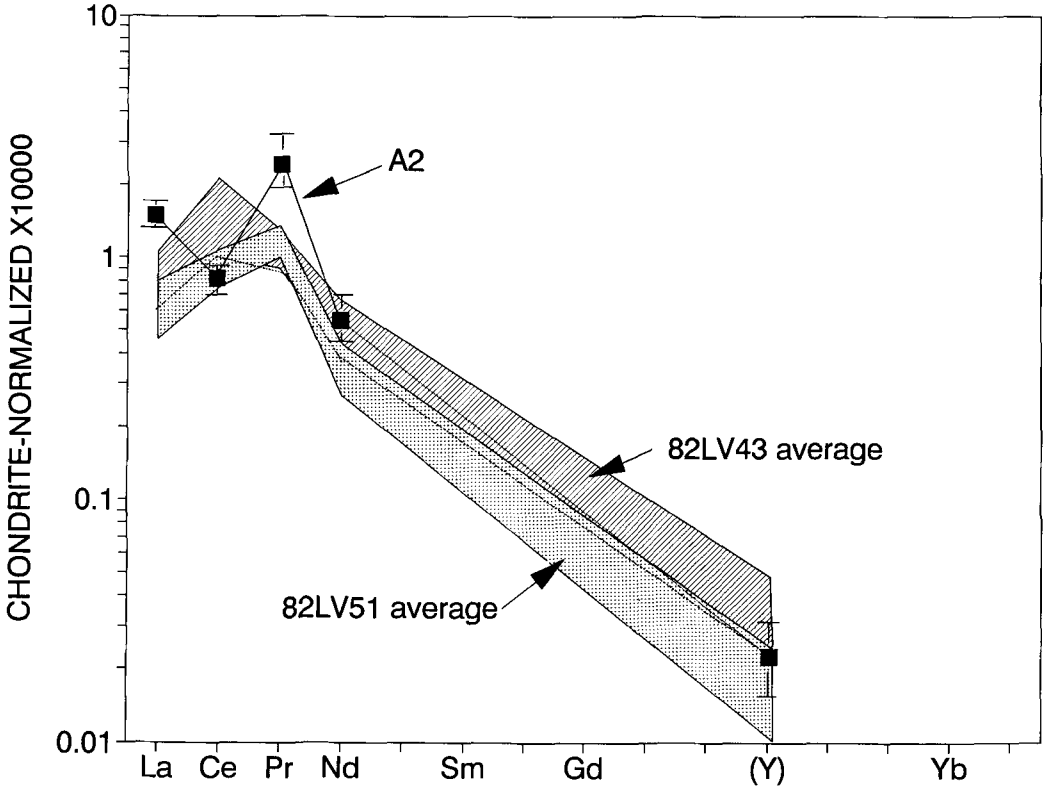

FIG. 7. Chondrite-normalized rare earth element distribution ratios for pyrochlores 82LV43 (ruled area is average of four analyses in Table 1) and 82LV51 (shaded area is average of seven analyses, excluding A2, in Table 1); A2 is shown separately, with error bars indicated.

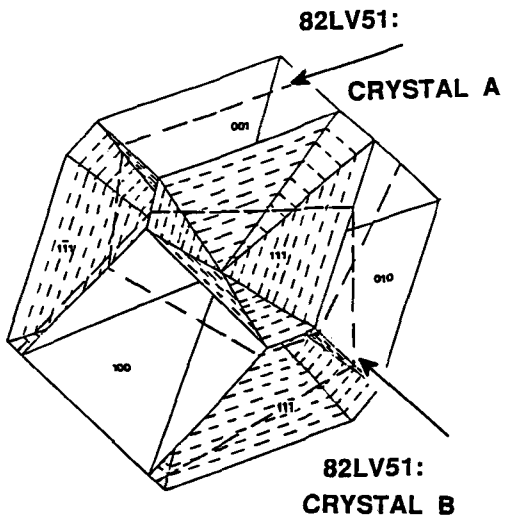

FIG. 8. Schematic 3-D model of the sector zones in pyrochlore crystals from 82LV51, showing the orientations of crystals in Figs. 2 and 3.

possess sector zonation, irrespective of whether or not they display octahedral faces. Thus neither elemental diffusion kinetics, localized magma heterogeneities, nor crystal-axis growth rate differentials, provide processes for developing sector zoning in these cubo-octahedral minerals.

Protosite formation has been suggested as an alternative mechanism of developing sector zonation in magmatic pyroxenes (Nakamura, 1973; Nakamura and Coombs, 1973). This process requires the partly formed structural sites, the protosites, to differ on the various crystal faces. The incomplete coordination sphere of the protosite imparts flexibility, and consequently the protosities that are able to vary most from the equilibrium position, are more effective at accommodating atoms not usually favoured by the completed structural site.

We suggest that the well defined sector zonation and cubo-octahedral faces developed because, with the coupled substitutions discussed above, growth was influenced by the difference between the protosite geometry and activity on cubic and octahedral faces.

Conclusions

(1) The variation in the chemistry of the pyrochlore crystals investigated reveals two site substitutions:

16*d* (*A*) site: Ca for U + Na,

and

16*c* (*B*) site Zr for Ti.

Although these two substitutions are coupled to balance cell size, it is not clear how the unit cell charge balance is maintained.

(2) Elemental distribution maps of pyrochlore from two carbonatites show that these minerals display concentric and oscillatory rhythmic zonation. In addition, sector zonation is observed that has not previously been recorded in pyrochlore.

(3) The cryptic concentric zonation apparently records element depletion in the host magma during pyrochlore growth, particularly of U, Ti and Zr. The rhythmic zonation indicates repetition of replenishment of the conjugate fluid, probably by circulation in a magma chamber or possibly by gravitational crystal settling, prior to renewed growth and element depletion.

(4) There were significant differences between the protosites on octahedral and cubic faces of the pyrochlore crystals that grew in the parent magma chamber to the Camile dyke. The different activities of these protosites in the localized physical and chemical conditions of the magma chamber during emplacement, were sufficient to influence site substitutions, leading to the development of the cryptic sector zonation.

Acknowledgements

We are indebted to Dr. D. D. Hogarth for his unstinting assistance throughout this study, to Dr. M. J. Norry for his constant encouragement, and to Dr. P. Henderson for arranging use of the British Museum (Natural History) microprobe. Dr. T. Williams and R. N. Wilson are thanked for technical assistance, and Dr. D. Mudge and J. Madden for their critical reading of early drafts of this script.

References

Borodin, L. S. and Nazarenko, I. I. (1957) Chemical composition of pyrochlore and diadochic substitutions in the $A_2B_2X_7$ molecule. *Geochemistry*, **4**, 278–95.

—— Bykova, A. B., Kapitonova, T. A., and Pyatenko, Yu. A. (1960) New data on zirconolite and its niobium variety. *Dokl. Acad. Sci. USSR., Earth Sci.*, **134**, 1022–24.

Gold, D. P. (1967) The minerals of the Oka carbonatite and alkaline complex, Oka, Quebec. *Proc. 4th Gen. meeting. Intern. Mineral. Assoc. India*, 109–25.

Hodgson, N. A. (1985) *Carbonatites and associated rocks from the Cape Verde Islands*. Ph.D. thesis, University of Leicester.

Hogarth, D. D. (1977) Classification and nomenclature of the pyrochlore group. *Am. Mineral.*, **62**, 403–10.

—— (1989) Pyrochlore, apatite and amphibole: distinctive minerals in carbonatite. In *Carbonatites: genesis and evolution* (Bell, K., ed.). Unwin Hyman, London, 89–104.

Kesson, S. E. and Ringwood, A. E. (1981) Immobilization of sodium in SYNROC. *Nuclear and Chemical Waste Management*, **2**, 53–5.

Knudsen, C. (1989) Pyrochlore group minerals from the Qaqarssuk carbonatite complex. In *Lanthanides, Tantalum and Niobium* (Moller, P., Cerny, P., and Saupe, F., eds.), Springer Verlag, 89–99.

Kuz'menko, M. V. (1984) Aspects of the systematics and typical chemistry of tantaloniobates of the pyrochlore group. In *Tipokhimizm Mineralov Granitnykh Pegmatitov* (Kuz'menko, M. V., ed.), IMGRE, Moscow, 5–32. (in Russian).

Le Bas, M. J. (1984) Oceanic carbonatites. In *Kimberlites 1: Kimberlites and related rocks* (Kornprobst, J., ed.), Elsevier, Amsterdam, 169–78.

Lebedeva, S. I., Bytov, V. P., Dubakina, L. S., and Yurkina, K. V. (1973) Microprobe determinations of the mode of deposition of trace elements in zircon-bearing pyrochlores and hatchettolites. In *Issledovaniya v oblasti rudnoi mineralogii* (Bezsmertnaya, M. S., ed.), Nauka, Moscow, 133–45 (in Russian).

McMahon, B. M. and Haggerty, S. E. (1979) Oka carbonatite complex: magnetite compositions and the related roles of titanium in pyrochlore. In *Kimberlites, Diatremes and Diamonds: their geology, petrology and geochemistry* (Boyd, F. R., Meyer, H. O. A., eds). Am. Geophys. Union. Wash. D.C. 382–92.

Nakamura, Y. (1973) Origin of sector-zoning of igneous clinopyroxenes. *Am. Mineral.*, **58**, 986–90.

—— and Coombs, D. S. (1973) Clinopyroxene in the Tawhiroko tholeiitic dolerite at Moeraki, north eastern Otago, New Zealand. *Contrib. Mineral. Petrol.*, **42**, 213–28.

Perrault, G. (1968) La composition chimique et la structure crystalline du pyrochlore d'Oka, P. Q. *Can. Mineral.*, **9**, 383–402.

Petruk, W. and Owens, D. R. (1975) Electron microprobe analyses for pyrochlores from Oka, Quebec. ibid., **13**, 282–5.

Serralheiro, A. (1968) *Formacoes sedimentares do arquipelago de Cabo Verde*. Junta de Investigacoes do Ultramar, Lisboa, 22pp.

Silva, L. C. and Figueirdo, M. O. (1980) Note on the occurrence of niobium-rich zirconolite in carbonatitic rocks of Santiago island (Cape Verde Republic). *Garcia de Orta, Ser. Geol.*, **4**, 1–6.

Treiman, A. H. (1989) Carbonatite magma: properties and processes. In *Carbonatites: genesis and evolution* (Bell, K., ed.). Unwin Hyman, London, 89–104.

—— and Schedl, A. (1983) Properties of carbonatite magma and processes in carbonatite magma chambers. *J. Geol.*, **91**, 437–47.

Vronskii, A. V. and Basina, V. A. (1963) Use of X-ray photography for the study of zoned pyrochlore. *Nauchnye Trudy Irkutskii Gosudarstvennyi Nauchno – Issledovatel'skii Institut Redkikh Metallov.*, **11**, 44–7 (in Russian).

Wass, S. Y. (1973) The origin and petrological significance of hour-glass zoning in titaniferous clinopyroxene. *Mineral. Mag.*, **39**, 133–44.

Woolley, A. R. and Kempe, D. R. C. (1989) Carbonatites: nomenclature, average chemical compositions, and element distributions. In *Carbonatites: genesis and evolution* (Bell, K., ed.), Unwin Hyman, London, 1–14.

[*Manuscript received 29 May 1991: revised 18 August 1991*]